3D Crust and Uppermost Mantle Structure beneath Tian Shan Region from Ambient Noise and Earthquake Surface Waves

Xiao Xiao[1] (xiaox17@mail.ustc.edu.cn), Lianxing Wen[2,1]

1. Laboratory of Seismology and Physics of Earth's Interior; School of Earth and Space Sciences, University of Science and Technology of China
2. Department of Geosciences, Stony Brook University

1. INTRODUCTION

As a typical active intracontinental mountain range in Central Asia, Tian Shan Mt. serves as the prototype in studying geodynamic processes and mechanism of intracontinental mountain building (Fig. 1). Under Tian Shan Mt. and nearby area, there are three main geological blocks, named as Tarim basin, Tian Shan Mt. and Junggar basin. To figure out underground structure and geological evolution history there, we study 3D crust and uppermost mantle structure beneath Tian Shan Mt. and adjoin region using joint surface wave tomography method based on ambient noise and teleseismic records.

2. DATA AND METHOD

My dataset contains records from 60 brand-band seismic stations, mainly locating at foot of Tian Shan Mt. and adjoin area (Fig. 1). Several stations, situating at the southern foot of Altai Mt. and northern foot of Kunlun Mt., provide critical ray path coverage of Junggar amd Tarim basins. Our dataset includes continuous records of vertical components from 2015 to 2016 and teleseismic waveforms from 2013 to 2016. Magnitudes of these earthquakes are over 5.5 and their focal depths are shallower than 200 km.

We combine the group velocity dispersion curves measured from empirical green's functions (EGFs) and teleseismic surface waves, obtain lateral isotropic Rayleigh group velocity maps at different periods based on traditional surface wave tomography method and construct a 3D V_{sv} model down to about 70 km using Markov Chain Monte Carlo method (MCMC) (Fig. 2).
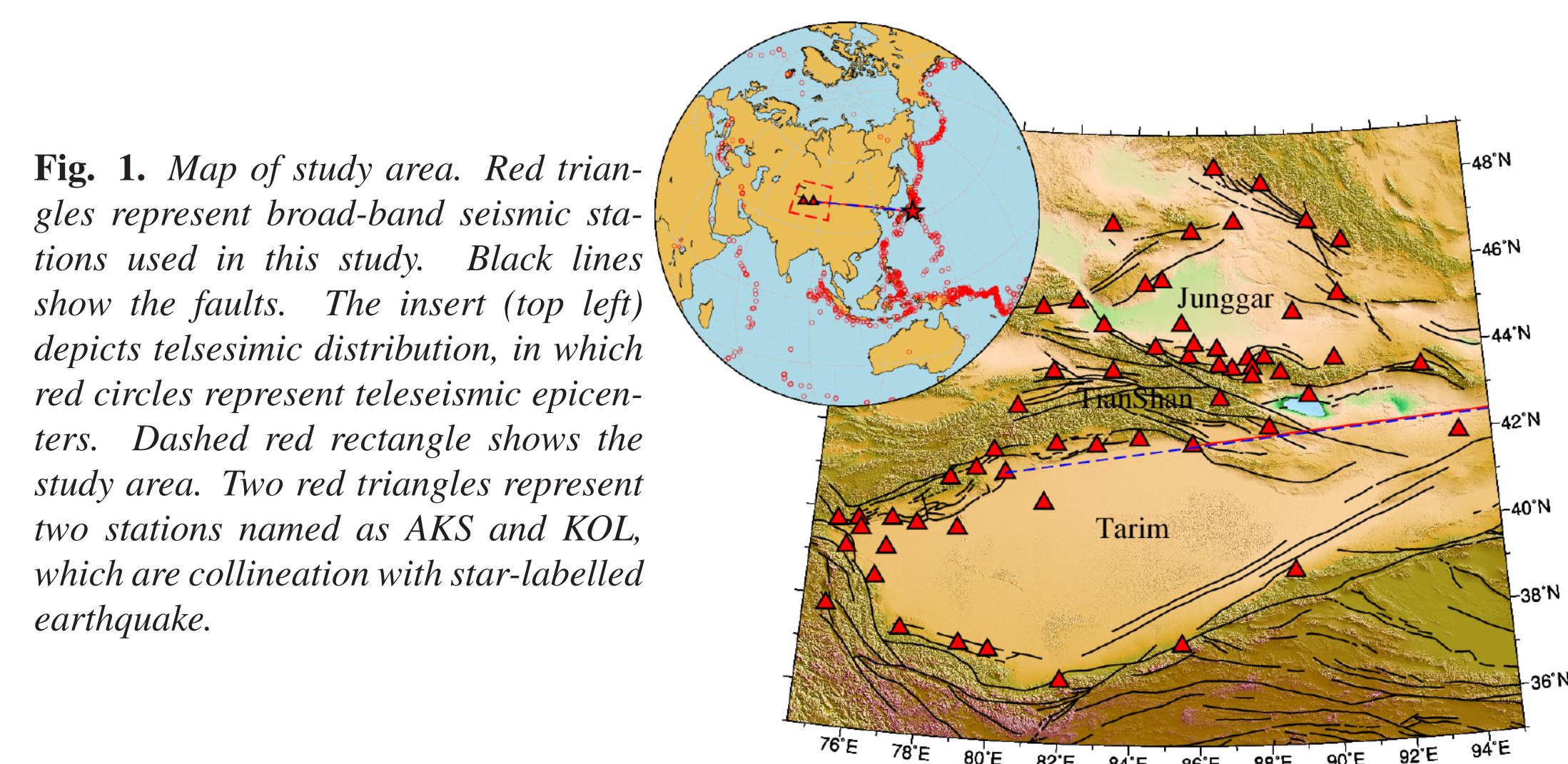

Fig. 1. Map of study area. Red triangles represent broad-band seismic stations used in this study. Black lines show the faults. The insert (top left) depicts teleseismic distribution, in which red circles represent teleseismic epicenters. Dashed red rectangle shows the study area. Two red triangles represent two stations named as AKS and KOL, which are collineation with star-labelled earthquake.

Fig. 2. Work flow of this study.
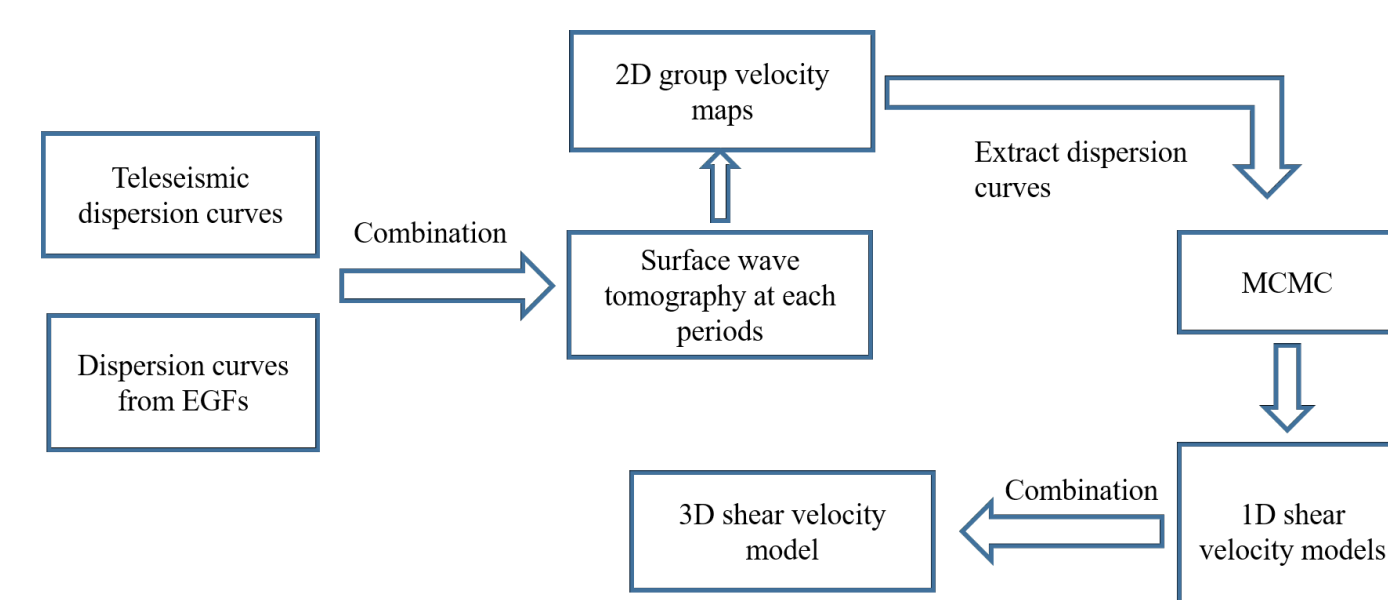
We control qualities of dispersion curves with spectral signal-noise-ratio (SNR) and standard deviation of measurements (Fig. 3). For EGFs, we define signal-noise-ratio (SNR) as ratio of peak in surface wave signal window and root mean standard (rms) in noise window at each period and we measure dispersion curves every trimesters , which provide standard deviation of dispersion curve between a pair of stations. We measure dispersion curves from telesemic waveforms of different events with two-station method. These curves give final dispersion curve with their medians and standard deviations at each periods .

We take averages of reliable dispersion curves, measured from EGFs and teleseismic waveforms to be final usable dispersion curves (Fig. 4) which are weighted by inverses of their standard deviations. The standard deviations of final dispersion curves are the summation of those constituents.
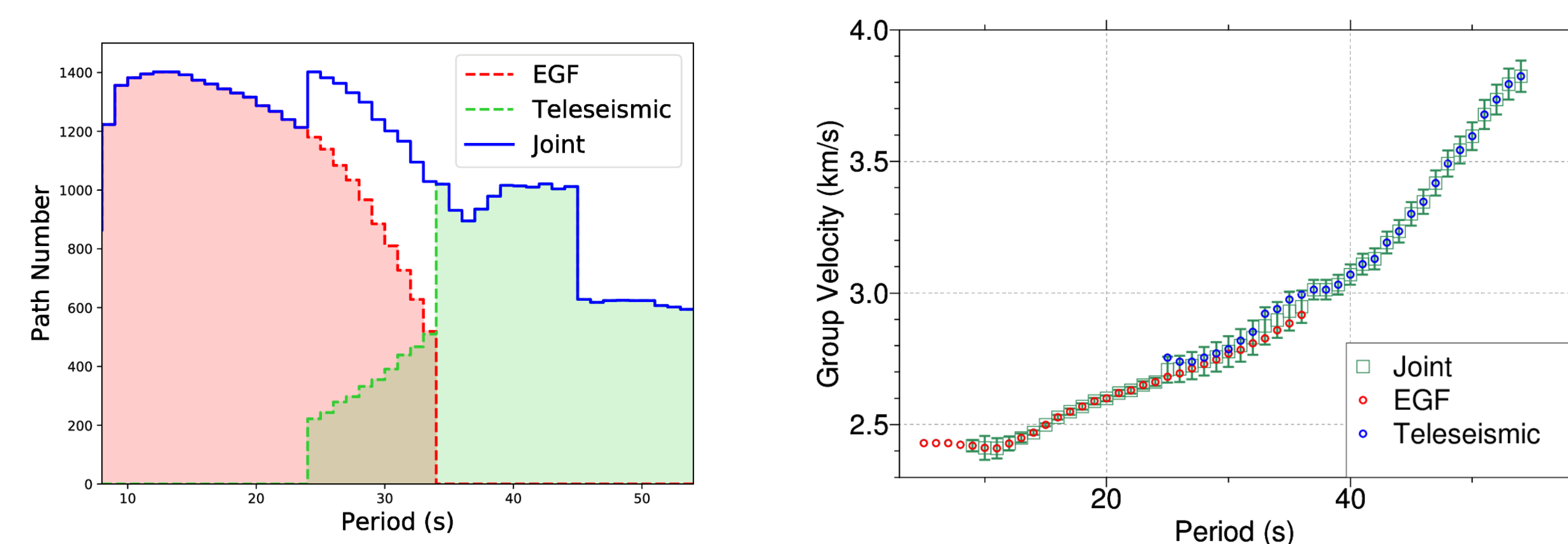

Fig. 3. Number variation of dispersion curves used for tomography due to dispersion curves quality control. The dashed limegreen line and corresponding limegreen area show number of used dispersion curves measured from teleseismic waveforms with two-station method while dashed red line and area denote number of those measured from EGFs at each period. The solid blue line indicates number of all dispersion curves which are summation of above two.
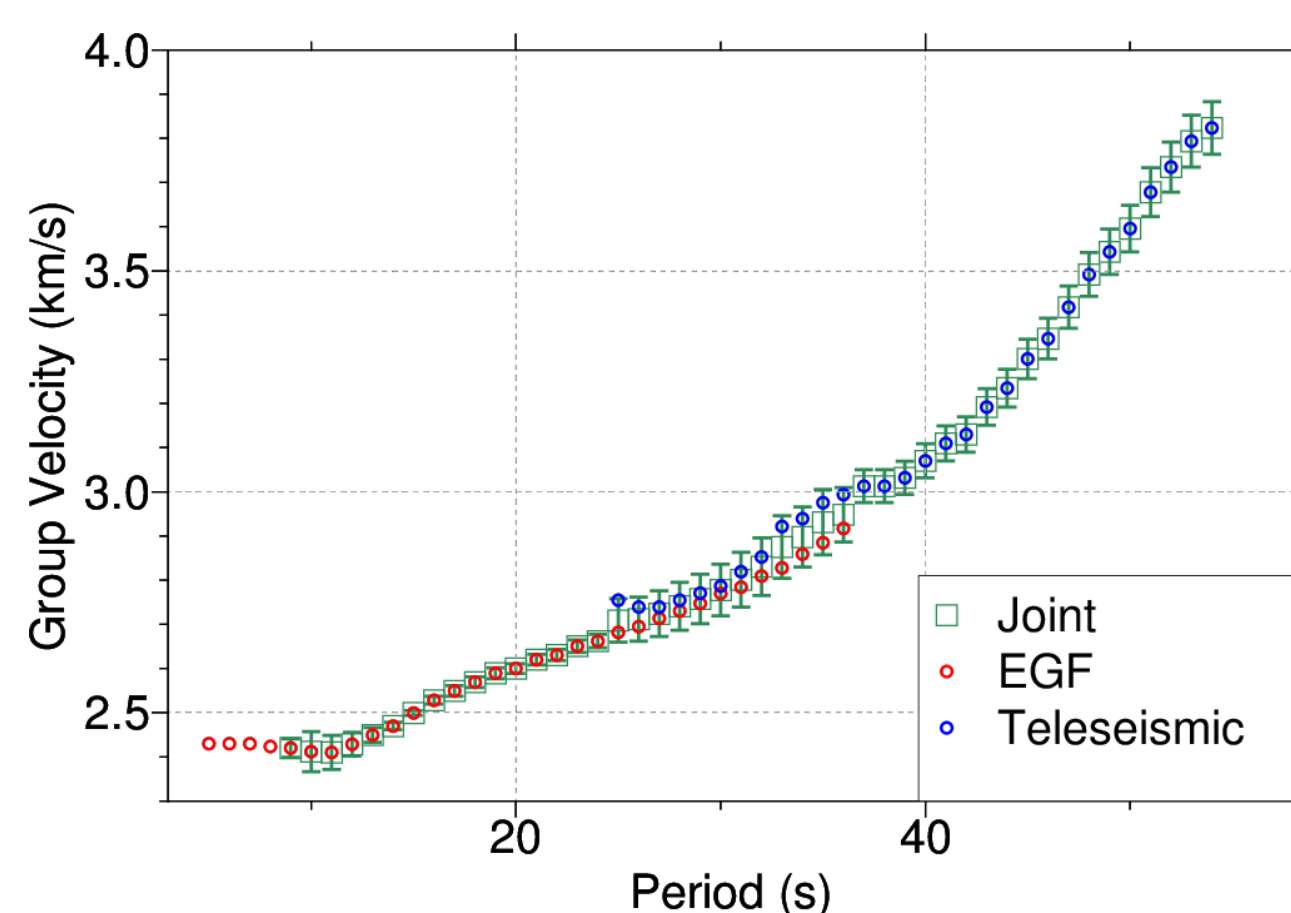
Fig. 4. Demo of group velocity dispersion curve combination between two stations, AKS and KOL. Red circles denote dispersion points measured from EGF while blue circles represent those estimated from teleseismic waveforms. Limegreen squares give combined dispersion curve. At overlap periods, green squares are weighted averages of blue and red circles , in which weights are inverses of their observational error and summation of their errors gives measurement error of combined dispersion curve.

3. 2D GROUP VELOCITY MAPS

With combined dispersion curves, we use traditional surface wave tomography method to image 2D Rayleigh group velocity maps.

Resolutions shown by fitted radius are consistent with those shown in checkerboard tests, indicating we can resolve 222 km × 222 km anomalies at Junggar basin, middle Tian Shan Mt. and western Tarim basin. However, at the main part of Tarim basin , eastern and western parts of Tian Shan Mt., we can only resolve 555 km × 555 km anomalies (Fig. 5).

2D Rayleigh group velocity perturbation maps partly show differences between three main geological blocks. At short periods (10, 26 and 33 s), perturbation maps are influenced by sedimentary layer, showing low group velocities in Junggar and Tarim basins. Long period map shows high velocities there, as they are cratons (Fig. 6).
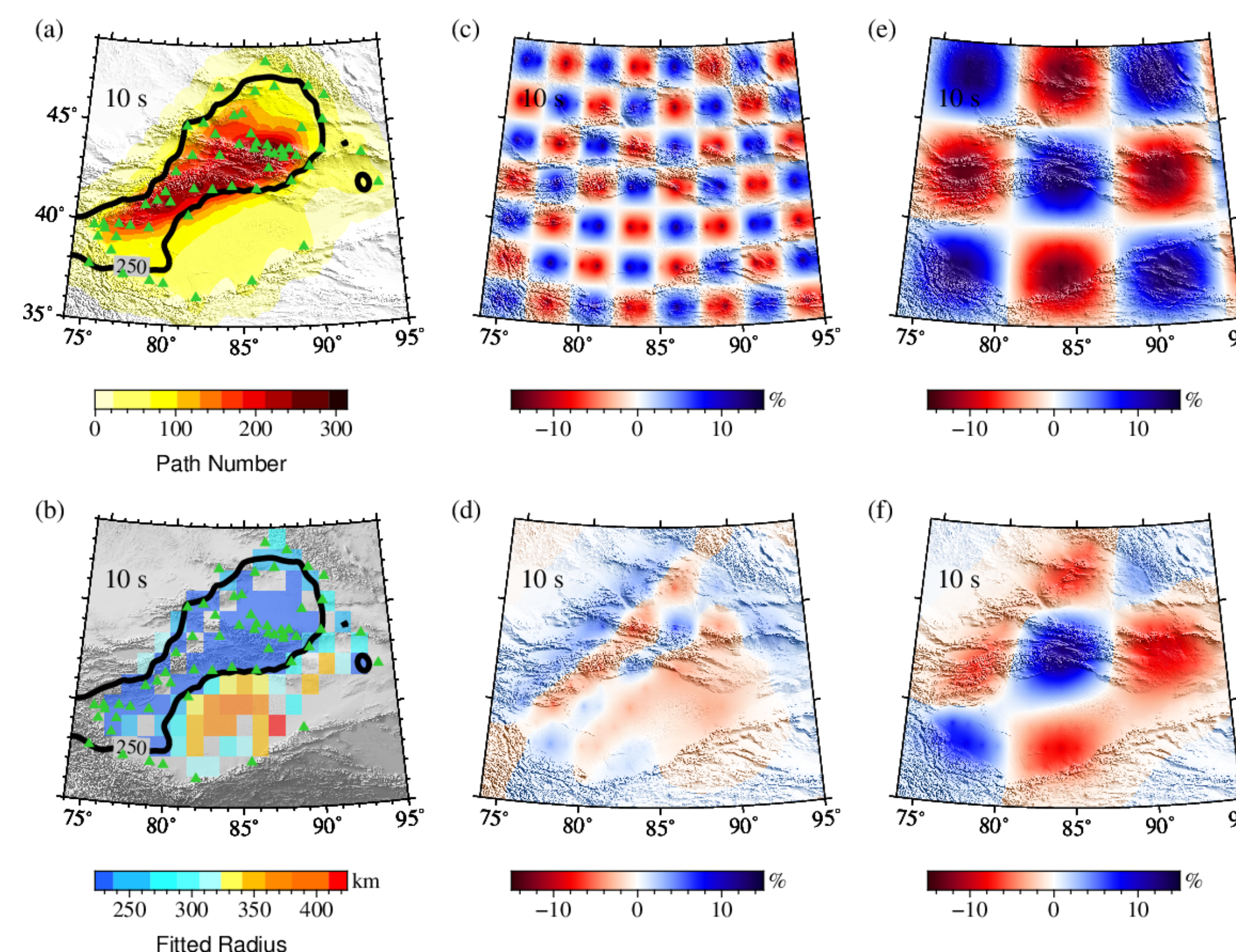

Fig. 5. Resolution analysis for Rayleigh group velocity tomography at 10 s. (a) Distribution of path density, indicating path numbers crossing each 1° × 1° cells. (b) Distribution of radius, which are fitted from resolution matrix. In panel (a) and (b), solid black line encloses area with resolution better than 250 km. Limegreen triangles indicate locations of seismic stations. Panels (c), (d) , (e) and (f) show inputs and outputs of checkerboard tests. They show Rayleigh group velocity perturbation maps, refering to 2.69315 km/s which is estimated average group velocity of study area at 10 s and the colorbars indicate percent of perturbation. Synthetic model (c) with 222 km × 222 km anomalies for checkerboard test and its recovered model (d). Increasing scale of anomalies up to 555 km × 555 km, we obtain synthetic model (e) and recovered one (f).
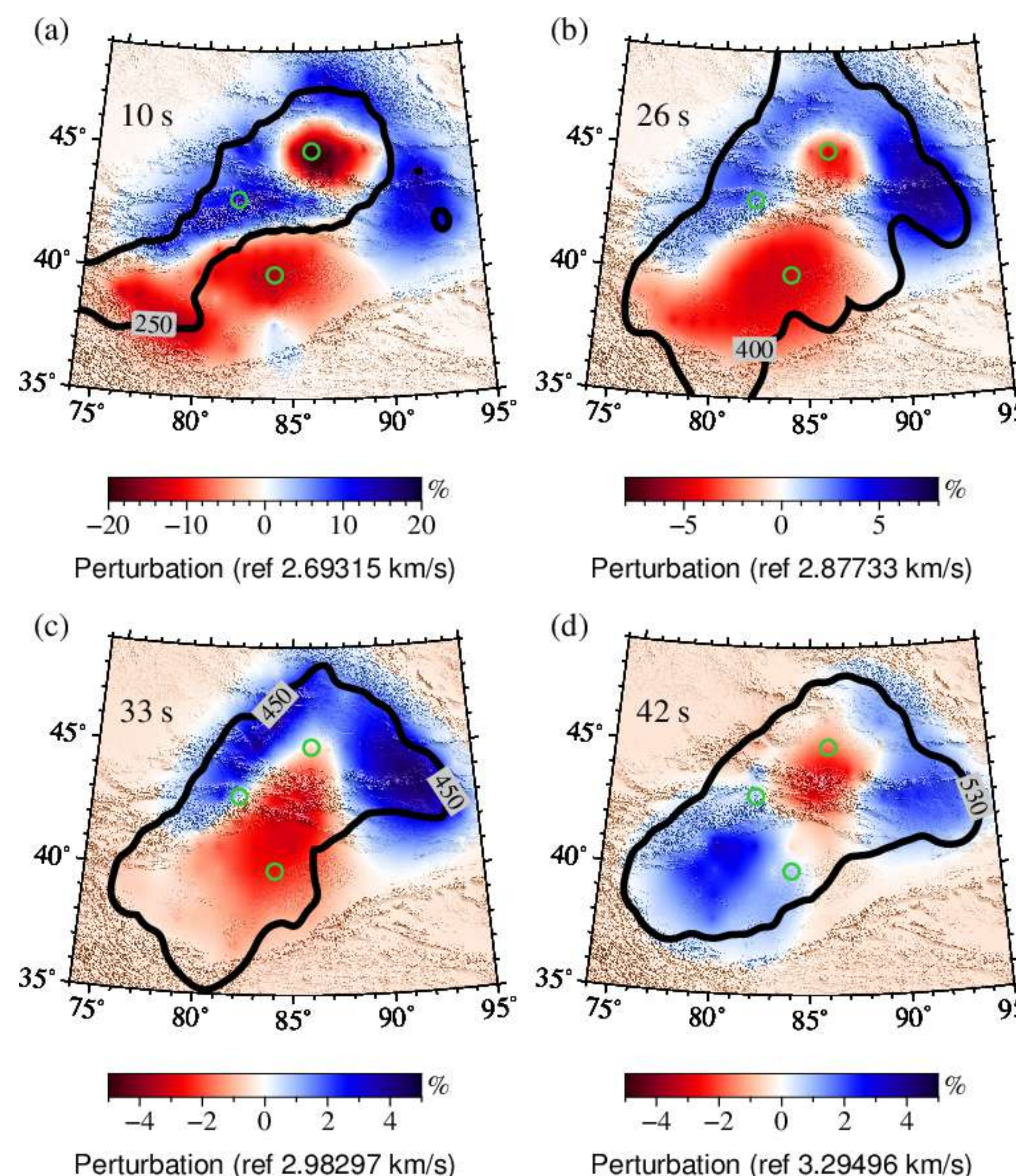

Fig. 6. Rayleigh group velocity perturbation maps at periods 10, 26, 33 and 42 s. The colorbars indicate percent of perturbation, refering to the velocities denoted in round brackets, which are averages of Rayleigh group velocities in study area at each periods, written at topleft of each panel. The solid black lines encloses main area with resolution better than annotated values. Three circles represent representative points of Tarim basin, Tian Shan Mt. and Junggar basin, separately, where 1D shear velocity models are inverted later.

4. SHEAR WAVE VELOCITY MODELS

We invert 1D shear velocity model at each points with Markov Chain Monte Carlo (MCMC) method, based on dispersion curves extracted from above 2D group velocity maps (Goutorbe, 2015).
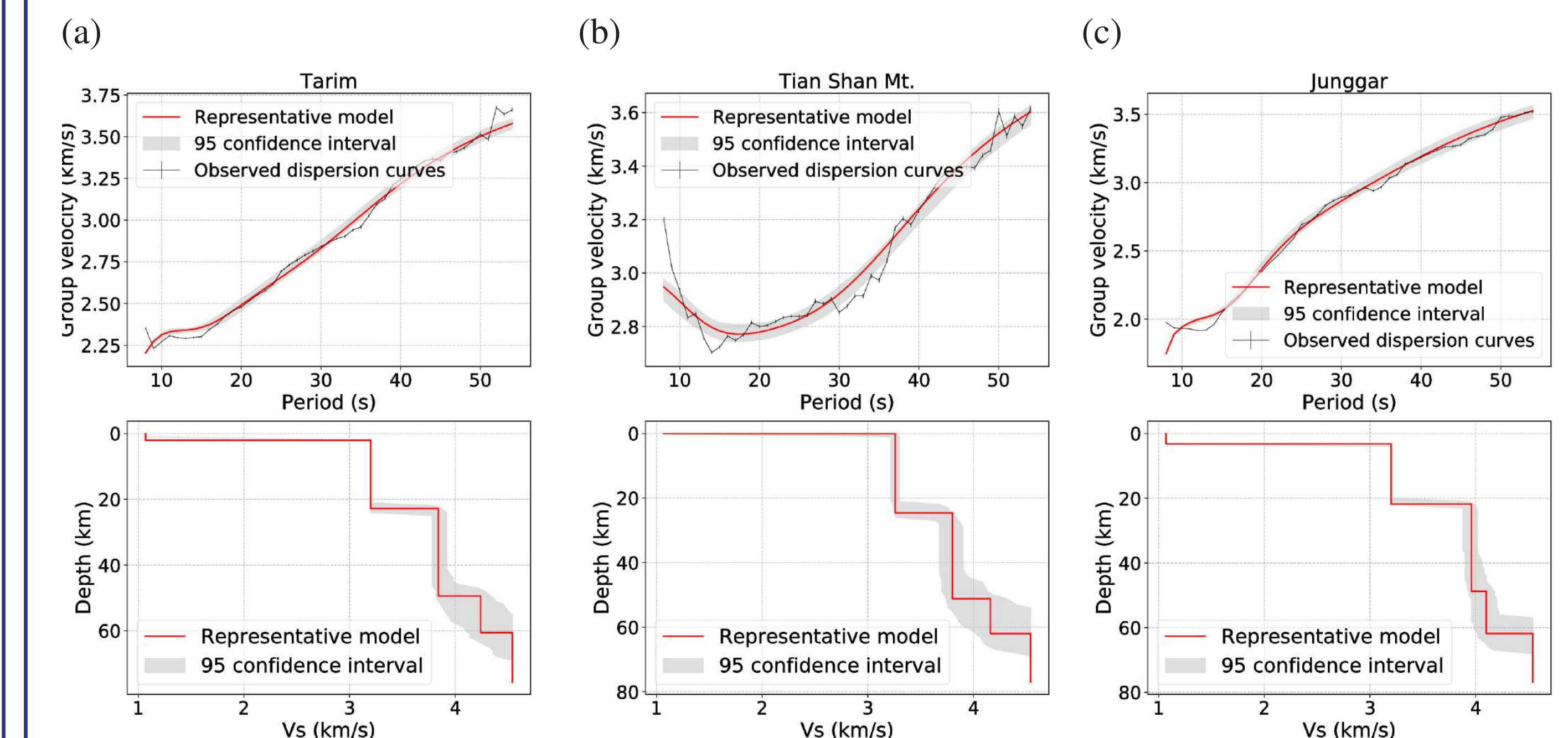

Fig. 7. Inverted 1D models at three representative points, locating at Tarim basin, Tian Shan Mt. and Junggar basin, separately. Observed dispersion curves (solid black lines with error bars) are extracted from previous 2D Rayleigh group velocity maps. Shade areas show the 95 percent confidence interval of the shear velocity models (below) and corresponding theoretical group velocity dispersion curves (upper). Red lines depict representative shear velocity models (below) and their synthetic dispersion curves (upper), which are cloesest to the average of all randomly sampled models at each point.
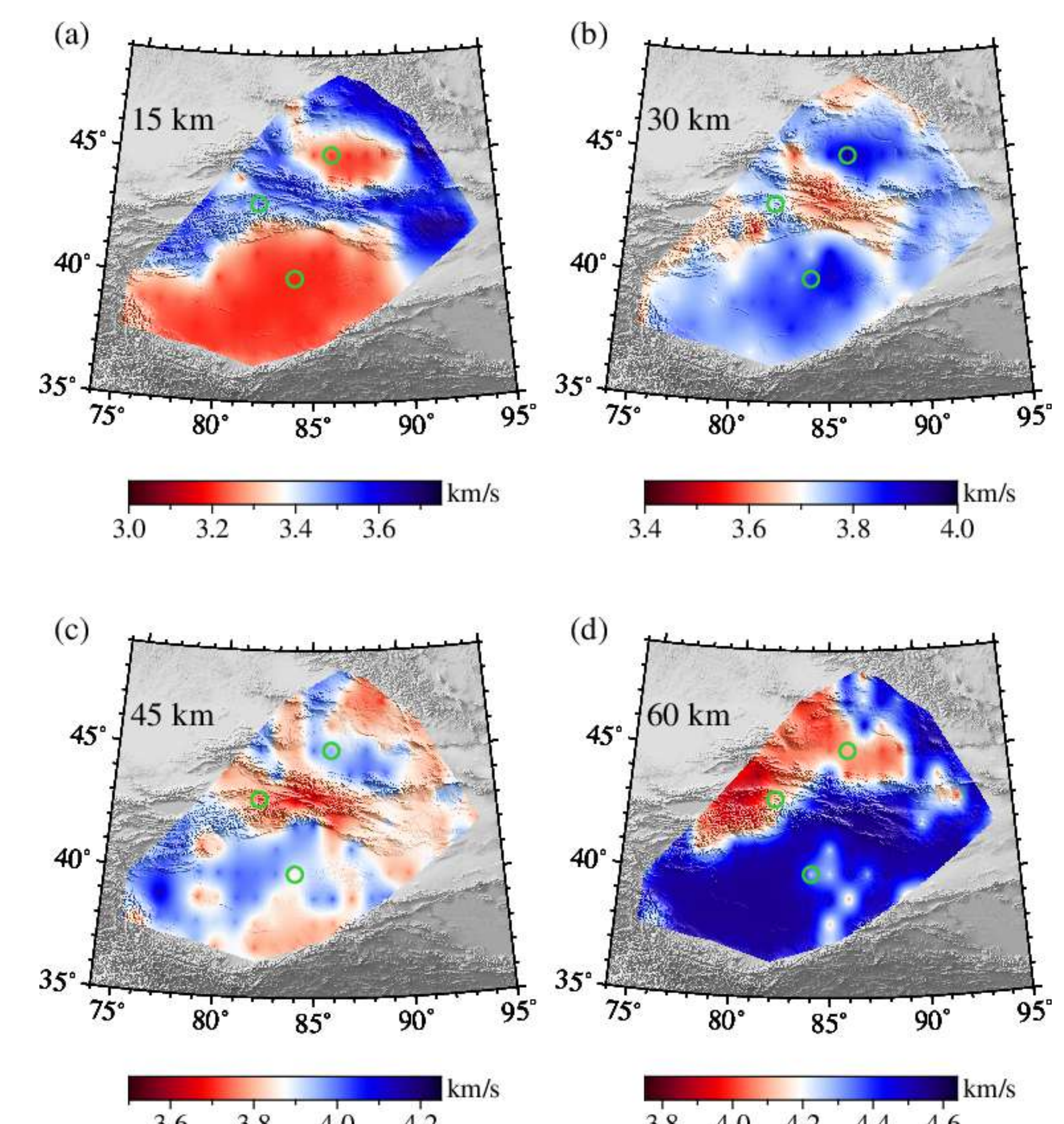

Fig. 8. Shear wave velocity maps at depths 15 , 30, 45 and 60 km. The green circles show locations of previous representative 1D shear wave velocity models. Study area is divieded to path covered part (colorful area) and that without coverage (dark gray area).

5. CONCLUSIONS

Current model has multiple resolutions at diffferent regions. It has 222 km × 222 km, or even better resolution at Tian Shan Mt. and Junggar basin and around 555 km × 555 km resolution due to sparseness and nonuniform data coverage at the main part of Tarim basin.

However, it does reflect difference between Tarim, Junggar basins and Tian Shan Mt.. The Tarim and Junggar basins correspond to low shear velocity in upper crust due to sedimentation and Tian Shan Mt. has high velocity. Things take on the opposite side in middle and lower crust due to the existence of cratons.

6. REFERENCES

Goutorbe, Bruno, Diogo Luiz de Oliveira Coelho, and Stéphane Drouet. "Rayleigh wave group velocities at periods of 6–23 s across Brazil from ambient noise tomography." Geophysical Journal International 203.2 (2015): 869-882.